CHAPTER 5

EXPERIMENTAL

The diffusion behaviour of aluminium in the semiconductors silicon (Si), germanium (Ge), gallium arsenide (GaAs), indium phosphide (InP) and indium antimonide (InSb) was investigated by nuclear resonance analysis (NRA). The sample preparation from these materials is described in chapter 5.1., followed by a short description of the implantations that were performed. The annealing system as well as the analysing set-up are described. A summary of the automatic energy scanning system installed at the University of Pretoria is followed by a description of the (p,γ) reaction used for this work. A short summary of the channeling technique concludes this chapter.

5.1. SAMPLE PREPARATION

The surface of the investigated semiconductors had to be cleaned before they were implanted and before the thin aluminium films were deposited. The different semiconductors were cleaned and prepared as described in the following sub-chapters.

A successive heating of the same sample for investigation of the diffusion behaviour might influence the results by leading to difficulties in the reproducibility that might arise due to several heating and cooling cycles. Therefore larger pieces of every semiconductor were implanted or prepared by vapour deposition. Samples of about 5 x 5 *mm* were cut from these pieces. This ensures that all samples of a semiconductor are prepared in the same way for an experiment.

For every annealing temperature a different sample was annealed to exclude effects that could occur from multiple heating and cooling of the same sample. Another advantage of this annealing method is the possibility to check obtained results by repeating the annealing experiment with a sample that is prepared in the same way.

5.1.1. SILICON

The surface of a float-zone (FZ) Si <100> and a Si <111> B^+ - doped wafer was etched with a 2 % HF water solution in order to remove the oxide layer. Half of this wafer was immediately transferred into a vacuum system for deposition of the t = 20 *nm* aluminium film with a resistive evaporation technique.

For every annealing experiment two samples cut from this wafer half were placed into a quartz tube with the aluminium sides facing each other in order to prevent evaporation of aluminium during the annealing process (sandwich - method). The annealing system is described in chapter 5.3.

The remaining wafer half was cut in two and one of the quarters was implanted at room temperature, the other quarter at 250 °C. Samples were cut from these quarters after implantation for subsequent annealing for one hour in vacuum at T_a = 500, 700 and 900 °C. During the annealing process the samples were not covered in order to avoid interdiffusion of the implanted aluminium samples.

5.1.2. GERMANIUM

A <111> n-type germanium crystal of the size 25 x 25 x 1 mm was mechanically polished and chemically cleaned with HNO_3 and placed into a vacuum system. A t = 13 *nm* aluminium film was deposited onto the polished surface of half of this crystal with a resistive evaporation method. Samples were cut from this crystal with a diamond saw and annealed for one hour in vacuum at T_a = 500 and 700 °C. The germanium samples were not covered during annealing because pits were observed on the surface after annealing samples with the sandwich method. These pits are diffusion channels that influence the diffusion behaviour dramatically.

The remaining polished germanium half was cut in two. One quarter was implanted at room temperature and the other at 250 °C. The samples cut from these pieces were also not covered during annealing for one hour in vacuum at T_a = 700 °C.

5.1.3. GALLIUM ARSENIDE

The surface of an undoped <100> gallium arsenide wafer was degreased in trichloroethylene (TCE) and isopropanol. Hereafter it was rinsed in deionised water and chemically etched in H_2O_2 : NH_4OH : H_2O (ratio 1 : 3 : 150) followed by another rinse in water. The oxide was removed in HCL : H_2O (ratio 1 : 1) followed by a final rinse in deionised water.

The wafer was cut in half. One of the halves was transferred into a vacuum system for the deposition of the t = 17 *nm* aluminium film with the resistive evaporation technique mentioned above. Samples were cut from this piece and subsequently annealed for one hour in vacuum at T_a = 450 and 550 °C. During the anneal the sandwich method described for silicon in 5.1.1.was applied.

The remaining cleaned wafer half was cut in two. One of the quarters was implanted at room temperature and the other at T_i = 250 °C. The samples cut from these were subsequently annealed for one hour in vacuum at T_a = 350, 450 and 550 °C. During the anneal the samples were not covered.

5.1.4. INDIUM PHOSPHIDE

An undoped *n*-type <100> InP wafer was degreased in hot trichlorethane, acetone and isopropyl alcohol (ratio: 1 : 1 : 1) and rinsed in methanol and deionised water. The wafer was cut in the middle and one half was placed in a vacuum system for deposition of a t = 10 *nm* aluminium film with the resistive evaporation method. Samples were cut from this half and subsequently annealed for one hour in vacuum at T_a = 300 and 400 °C using the sandwich method.

The remaining clean wafer half was cut in two. One of these quarters was implanted at room temperature, the other at T_i = 250 °C. Samples were cut from these quarters and annealed for one hour at T_a = 300 and 400 °C in a vacuum system. During annealing the samples were not covered.

5.1.5. INDIUM ANTIMONIDE

The surface of a tellurium doped *n*-type <110> InSb wafer was cleaned with CP4 for 5 seconds. CP4 consists of HF, HNO_3 and CH_3COOH (ratio: 3 : 5 : 3). After cleaning, the disc was rinsed in deionised water and dried with nitrogen. The wafer was cut in half.

One of the halves was placed in a vacuum system for deposition of a t = 10 *nm* aluminium film onto the surface with the resistive evaporation system. Samples cut from this wafer were annealed for one hour in vacuum at T_a = 250 °C with the sandwich method.

The other cleaned wafer half was cut in two. One of the quarters was implanted at room temperature, the other at T_i = 250 °C. These samples were not covered during annealing for one hour at T_a = 250 °C in vacuum.

5.2. IMPLANTATIONS

All implantations were performed at the Schonland Research Centre for Nuclear Sciences at the University of the Witwatersrand (WITS) in Johannesburg with a Varian-Extrion implanter. Due to implanter problems beyond our control the ion energy could not be measured directly. It was indirectly determined as 120 *keV* by comparing the experimentally observed implantation profiles with TRIM [14] simulations. However, it must be stressed that a knowledge of the exact ion energy is of no importance for our investigation. The fluence of the implantation was for all samples $5x10^{16}$ aluminium ions cm^{-2}.

The implantations at room temperature were performed with a beam current of about 1 μA which corresponds to a dose rate of 1 x 10^{13} ions $cm^{-2}\ s^{-1}$. This rate is low enough to avoid excessive heating of the samples.

Hot implantations were performed at 250 °C with a beam current of about 3.4 μA which corresponds to a dose rate of 3.4 x 10^{13} ions $cm^{-2}\ s^{-1}$. The temperature of the heated sample holder was measured on the surface close to the samples with a thermocouple. During the implantation the temperature was kept within ± 20 °C.

Samples were tilted during implantations at an angle of 7° relative to the surface normal to avoid channelling of the ions during implantation.

5.3. ANNEALING SYSTEM

The samples were annealed in a 60 cm long cylindrical oven. The maximum temperature of this oven is at $T = 1000$ °C, which is reached in the middle of the oven with a slight gradient towards the sides. A thermal sensor with a feedback system keeps the adjusted oven temperature within $\Delta T = \pm 5$ °C.

For the annealing process the samples were placed in quartz-glass tube connected to a vacuum system. A thermocouple was placed next to the samples inside the quartz tube to provide the actual temperature at the location of the samples. The oven was heated to the desired temperature before it was shifted over the quartz-tube. The vacuum was better than 10^{-7} mbar while the quartz tube with the samples was in the oven.

Slight adjustments to the annealing temperature could be made, by moving the oven relative to the quartz-glass tube by making use of the temperature gradient inside the oven.

5.4. THE ENERGY SCANNING SYSTEM

For obtaining depth profiles with NRA the energy of the incoming protons has to be changed in a controlled manner which is difficult to realise by setting the analysing magnet every time the energy has to be changed. This is due to hysteresis effects and difficulties in setting the magnet reproducibly within $\Delta E = 500\ eV$ of the desired energy. Therefore an energy scanning system is necessary to change the proton energy in small reproducible steps. Various scanning methods are employed world-wide. The system installed at the University of Pretoria is based on a principle developed by Amsel et al. [37-39]. The accelerator group of the National Accelerator Centre (NAC) in Faure made the appropriate adaptation for our accelerator. The system is designed for proton energies up to 2.5 MeV and is able to step through a total energy range ΔE of some 40-100 keV.

Displayed in Fig. 9. is a schematic layout of the accelerator beamline, where the energy scanning system is installed.

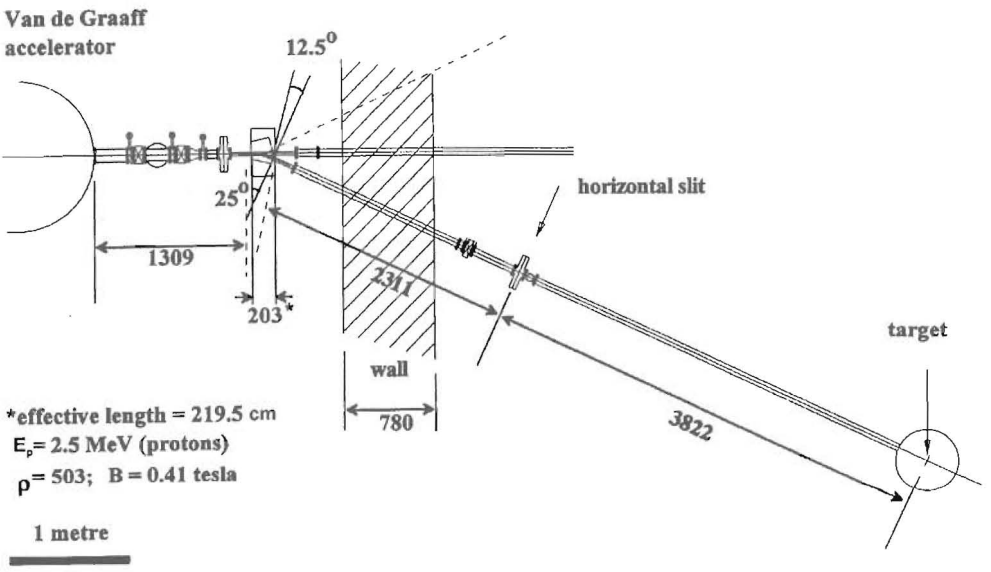

Fig. 9: Layout of the accelerator beamline in which the energy scanning system is installed.

The energy scanning system consists of two sets of electrostatic deflection plates. One set is located in front and the other one behind the switching magnet at similar, but not identical distances from the magnet. When a voltage is applied on the first set of plates the beam gets deflected from its original trajectory.

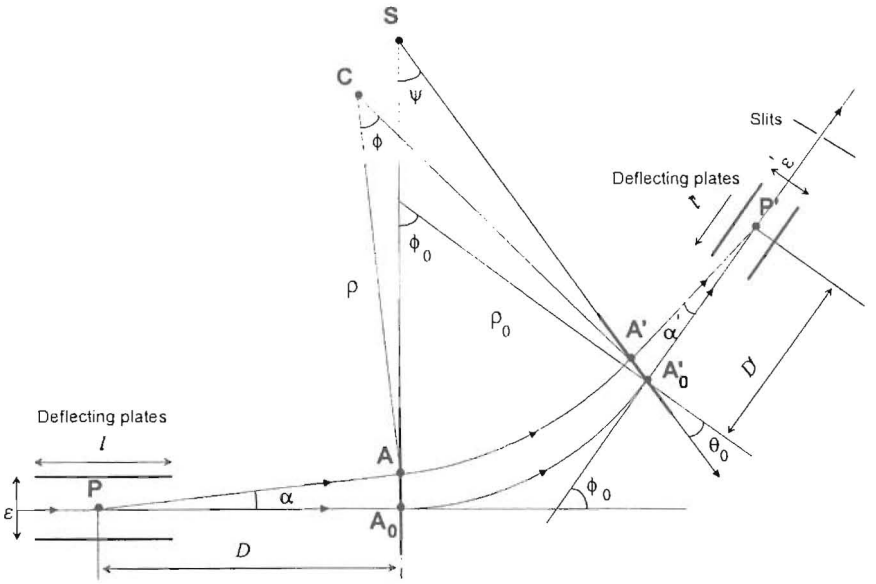

Fig.10: Schematic diagram of a set of deflection plates, together with the deflected and undeflected beam path.

The second set of deflection plates after the magnet has the opposite polarity of the first set of plates. This corrects the disturbed trajectory of the deflected particles in a way that the beam is now deflected onto the horizontal energy selection slits located downstream at the horizontal focus, which is schematically shown in Fig. 10. The feedback from the slits causes the stabilising system to increment the terminal voltage of the accelerator until the beam trajectory is passed through the slits. Detailed calculations for our system are in ref.[40].

By varying the applied voltage on the deflector plates it is easy to change the energy of the analysing ions without changing the setting of the analysing magnet. The energy variation without changing the magnetic field opens up the important possibility of running the experiment in a multi-sweep mode, since no hysteresis problems exist.

A Pentium computer controls the power supply for the deflector plates in front and behind the switching magnet. To automatically save a spectrum after a scan the PCA - Multiport can be run in a batch mode. An example for one of the batch programs, written for that purpose, is listed in Appendix A.

5.5. γ - RAY DETECTION

For the gamma ray detection from the nuclear reaction analysis two gamma detectors were used. One of the detectors is a 5.3 *cm* EG&G Ortec high-purity intrinsic germanium coaxial photon detector, the other a 5 *inch* Bicron NaI-scintillation detector.

When gamma radiation interacts with the NaI(Tl) crystal, the transmitted energy excites an iodine atom and raises it to a higher energy state. When the iodine atom returns to its ground state the energy is re-emitted in the form of a light pulse in the ultraviolet which is promptly absorbed by the thallium atom and re-emitted as fluorescent light. The efficiency of a NaI detector is high, however its resolution is relatively poor (peak width of 6 % at 1 *MeV*).

The coaxial intrinsic germanium detector consists of a cylinder of intrinsic germanium with impurity concentrations of less than 10^{10} atoms cm^{-3}. The core of this cylinder consists of doped germanium and the contact on the surface of the cylinder consists of lithium. Gamma radiation creates electron hole pairs in the active region (intrinsic germanium), and the charge

produced is collected under the influence of the bias voltage of 3000 *volts*. Germanium detectors have a resolution of about 0.15% at 1.3 *MeV*. However, due to the size of the germanium diode the counting efficiency of the germanium detector is poor. By adding the counts of both detectors (Ge and NaI) the counting efficiency was increased to reduce the analysing time to an acceptable level.

Through modified ports in the analysing chamber the two detectors could be positioned close to the target to reach a large solid angle $d\Omega \approx 10^{-1}$ *sterad* of detection. The two detectors and the incident beam are in the same horizontal plane. The angle between the beam axis and the NaI detector is $\theta_1 = 90°$ and between the Ge detector and the beam axis $\theta_2 = 127°$.

In Fig.11 a schematic drawing of the layout of the analysing detector system is shown.

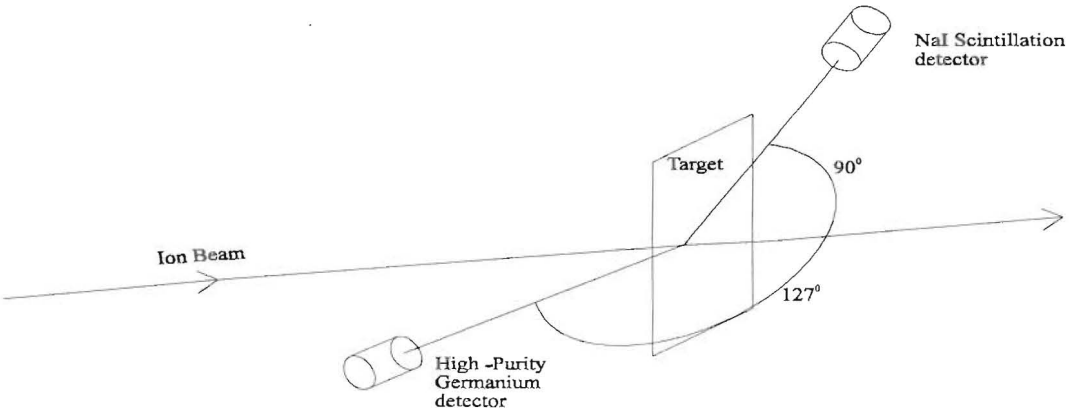

Fig.11: Detector configuration relative to the target and the incoming beam.

5.6. DATA AQUISITION

A block diagram of the electronic circuitry for data acquisition of NRA measurements is displayed in Fig.12. When a gamma ray arrives at one of the detectors the signal is amplified by a Tenelec TC243 amplifier. The output signal of each amplifier is sent to a single channel analyser (SCA). The logic output from the SCA is connected to an Ortec 433 sum-invert amplifier, which is a logic-or amplifier. The sum invert amplifier is set to non-invert, which ensures that when on either detector a gamma-ray in the desired energy window is detected a

logic pulse is given to the PCA-Multiport. This Tenelec multichannel analyser is set on multichannel scaler (MCS) mode.

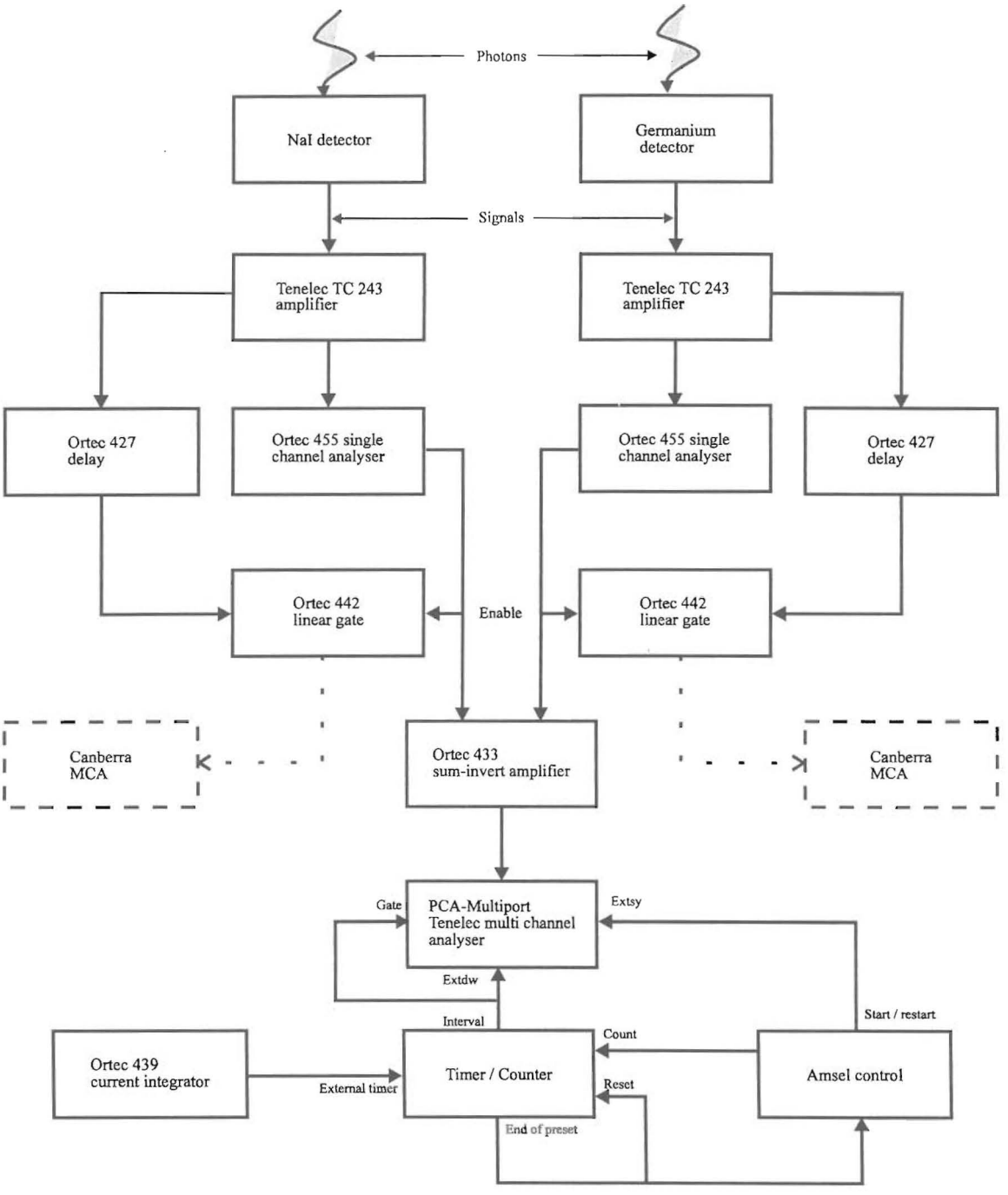

Fig.12: Block diagram of the electronic circuitry used for the NRA measurements.

5.6.1. SETTING OF ENERGY WINDOWS

Before NRA measurements are performed several adjustments and calibrations of the system have to be made. An energy window has to be set at the SCA to detect only γ-rays with energies that result from the employed nuclear reaction. The setting was performed separately for each detector with a radioactive ^{60}Co source, which has characteristic gamma rays at 1173 *keV* and 1332 *keV*. The amplified signal from the detector is send simultaneously through a Ortec 427 delay and the SCA to a linear gate. The logic signal from the SCA is connected to the gate to enable analogue pulses within the set energy window to pass to the multichannel analyser MCA (dotted line). The windows of the SCA are at this stage completely open to allow the full energy spectrum to pass and the delay is set to $\tau = 2\ \mu s$ to ensure that the signals arrive at the gate in coincidence.

Once the MCA was calibrated, the upper and lower levels of the SCA were adjusted to the desired energy window. The γ-rays from the ^{27}Al(p,γ)^{28}Si reaction have a maximum energy of 10.76 *MeV* (see chapter 5.7). Other γ-rays with lower energies from this reaction were not used for detection because of background problems. The energy windows were set differently for both detectors. The SCA energy window for the germanium detector was set between 10.3 *MeV* and 11.5 *MeV* and for the NaI detector an SCA energy window between 10.4 *MeV* and 11.4 *MeV* was set. The slightly smaller window for the NaJ detector was chosen because of its higher counting efficiency. With this setting of the SCA energy windows, the best signal to background ratio could be reached.

5.6.2. NRA MEASUREMENTS

The power supply for the energy scanning system (see chapter 5.4.) as well as the PCA Multiport used for the data acquisition are controlled by a Pentium - computer running the Turbo Pascal computer code AMSEL.

At the beginning of a NRA measurement the energy of the incoming proton beam is set to its starting value by the computer program, which also sets the PCA-Multiport to channel 1. After sending the starting pulse, counts from the SCA are collected into that channel until a certain predetermined charge was collected on the sample.

When the set charge is reached on the sample, the counter sends a feedback to the scanning system to increase the energy of the incoming proton beam. The counter for the integrated beam current is reset and the MCA-Multiport is set to the next channel. A start pulse results in counting gamma rays into that channel until the set charge on the sample is reached again.

This charge on the sample is measured with a counter that is connected to the digital output of the Ortec 439 current integrator. Within a measurement the value of the counter is set to a constant value to ensure that all the energy steps are performed for the same charge, e.g. the same amount of incident protons on the sample surface.

Secondary electrons of the analysing beam – target interaction are falsifying the measured beam current readout at the integrator. An aluminium plate with a hole for the analysing beam is connected to a negative potential of $U = -200\ V$ and placed about 1 *cm* before the target to suppress secondary electrons.

Up to 10 energy scans were performed for every measurement. The spectrum obtained after each scan was saved. This was done for several reasons. After about 10 scans a degradation of the surface due to the proton beam was observed. Some of the sample surfaces were flaking. Therefore the spectra taken after every scan were carefully compared to rule out flaking effects on the target surface that would influence the results.

Another reason for saving each scan was that the electricity supply for the system was not reliable. Long measurements were performed without attending to the accelerator. A power failure or a short power drop shuts down the power supply of the analysing magnet as well as the accelerator itself. However, saved spectra after a few scans contained already enough information about the depth profile.

5.6.3. MAGNET SETTING

The scanning system (see chapter 5.4.) scans the energy symmetrically about a central proton beam energy. The central energy together with the step width and the number of steps determines the proton energy region that is covered in a measurement. It is crucial for every

measurement to first calibrate the PCA – Multiport by setting the magnet correctly to the desired central energy.

For setting the analysing magnet of the accelerator a solid aluminium target was used. The spectrum was taken with the PCA-Multiport as described above. An example for such a calibration spectrum can be seen in Fig. 13. The 'step' represents the target surface, which, in the case of aluminium corresponds to incoming protons at 992 *keV*. The deflecting magnet was set to get this 'step' at about channel 15 of the PCA-Multiport for background corrections at lower proton energies.

The computer program was set to a proton energy step width of $\Delta E = 500\ eV$ for the implanted samples, which for example corresponds to a step width in silicon of 12.2 *nm*. To cover the implanted depth in the sample one scan contained 80 steps. For the in-diffusion analysis the step width was set to $\Delta E = 250\ eV$ which corresponds to 5.3 *nm* in aluminium and typically 40 steps were performed in a scan. A further description of the system can be found in [41].

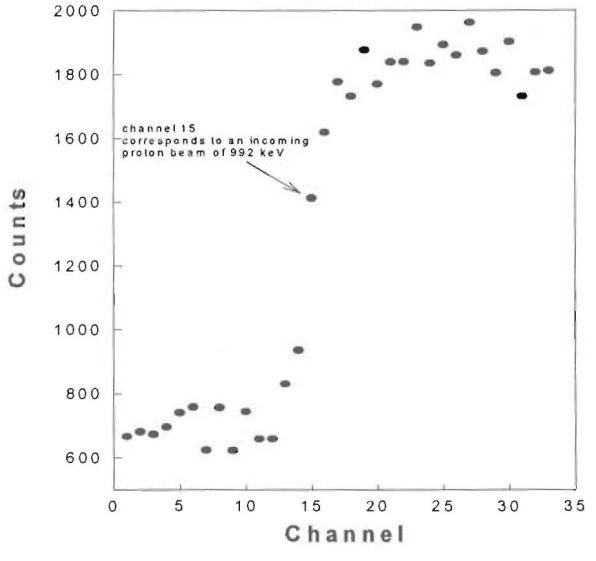

Fig. 13: Spectrum of a solid aluminium target for calibration purposes. Channel 15 corresponds to an incoming proton energy of 992 keV.

5.7. THE $^{27}AL(p,\gamma)^{28}SI$ REACTION

The reaction used for the depth profiling analysis is the $^{27}Al(p,\gamma)^{28}Si$ reaction at a proton energy of 992 *keV*. Aluminium has only one stable isotope: ^{27}Al which has at least 22 (p,γ)

resonances below 1 *MeV* [42]. All the resonances have a width smaller than 200 *eV*. The cross section is largest for 992 *keV* (σ = 31 *mb*) followed by 632 *keV* (σ = 5.3 *mb*).

Fig.14 shows a γ-ray spectrum of a thin aluminium sample for the 992 *keV* resonance used in this work recorded with a Ge(Li) detector [43].

The high-energy γ-rays result in three peaks each in the spectrum: full-energy peak, single-escape (*S.E.*), and double-escape (*D.E.*) peaks. The full-energy peak corresponds to the case, when the total energy of the γ-ray is absorbed in the detector. The escape peaks are observed, when one or both of the annihilation γ-rays (511 *keV*) are lost from the detector.

The decay scheme for this reaction, which has a width of ΔE_r = 105 *eV* [44], is presented in Fig.15 [45]. The excited level of silicon is at 12.542 *MeV* from where it decays by different decay modes to its ground state. The direct decay to the excited state at 1.78 *MeV*, resulting in a γ-ray with the energy 10.76 *MeV*, has with 78% the highest probability [46]. A direct transition to the ground state would be a *M3* transition and is therefore very unlikely.

One major advantage of this high γ-ray energy region is the low background yield and usually the lack of other interfering resonances of the target material. The only other possible reaction for ^{27}Al having a γ-energy within our SCA windows is for a proton energy at 632 *keV* resulting in a γ-energy at E_γ= 10.41 *MeV* with a cross section of 5.3 *mb*. However, when analysing silicon with a proton beam of 992 keV this would correspond to a depth of 9 μm in silicon whereas the aluminium is only implanted at a depth of 0.2 μm.

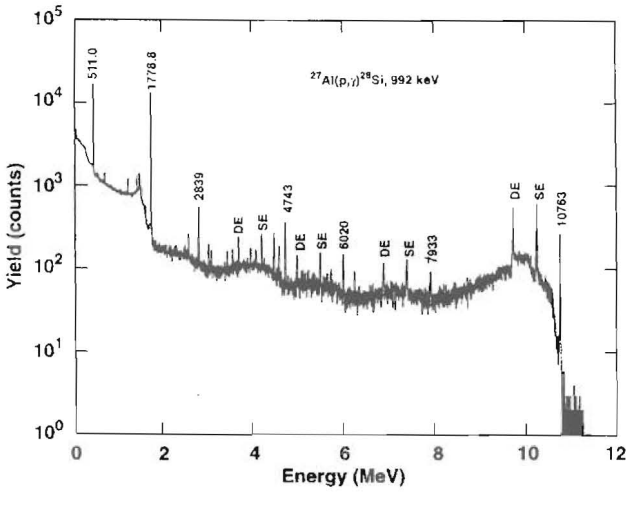

Fig.14: γ-ray spectrum for the 992 keV ^{27}Al(P,γ)^{28}Si resonance [43].

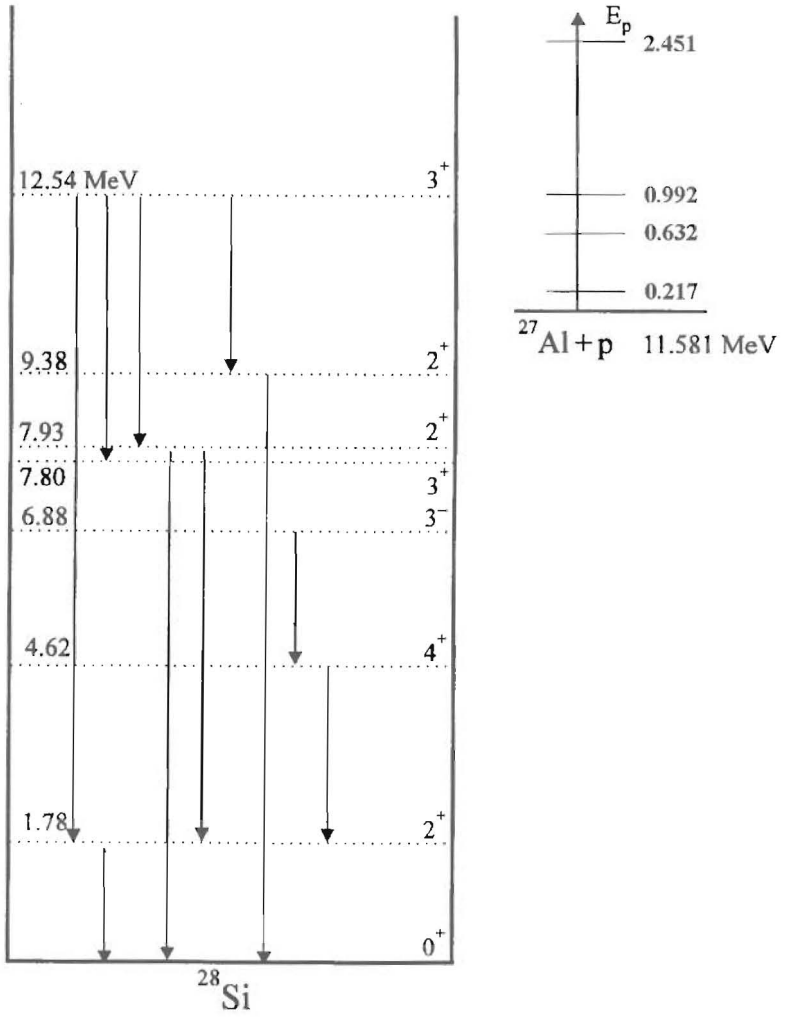

Fig.15: Decay scheme of the excited level of ^{28}Si at 12.542 *MeV* to the ground state.

5.8. CHANNELING

The steering of ions by lattice potentials in a crystal is known as channeling. Channeling of energetic ions occurs when the beam is carefully aligned with a major symmetry direction of a single crystal. A major symmetry direction is one of the open directions as viewed down a row of atoms in a single crystal. Channeled particles cannot get close enough to the atomic nuclei of the target to undergo large angle Rutherford scattering. Therefore the scattering of the substrate is drastically reduced. There is always a full interaction with the first monolayers of the solid, resulting in a surface peak in the spectrum. A schematic drawing of particle trajectories undergoing scattering at the surface and channeling within the crystal is shown in Fig. 16.

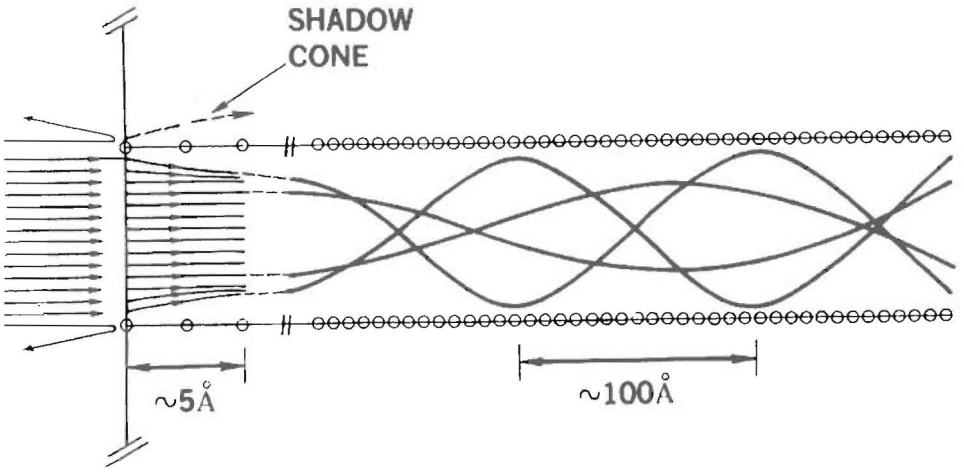

Fig. 16: Schematic of particle trajectories undergoing scattering at the surface and channeling within the crystal. The depth scale is compressed relative to the width of the channel in order to display the trajectories[47].

The trajectory of a channeled ion is such that the ion makes a glancing angle impact with the lattice axes (axial channeling) or planes (planar channeling). Detailed descriptions of the channeling effects as well as for its different applications are in refs. [48-52].

The channeling effect can be used for analysing crystal properties like for example the lattice site occupation of impurity atoms [53] or investigation of the crystalinity of a material. For this work the major interest was in analysing the damage introduced into the semiconductors during the aluminium implantation as well as how the crystal structure recovered during the different annealing steps. Having a disturbed lattice due to point or extended defects results in an increase in the backscattering yield of an orientated (aligned) crystal. Comparing an aligned backscattering spectrum of an unimplanted crystal with the aligned spectrum of an implanted crystal indicates the radiation induced damage introduced into the lattice during the implantation.

The channels from the backscattering spectra were converted to a depth scale by assuming an energy loss as found for an amorphous solid.

The channeling experiments were performed with the Van de Graaff accelerator at the University of Pretoria using 1.5 *MeV* α particles. The semiconductor samples were mounted on a three axis goniometer with an angular precision better than 0.1°. The silicon surface barrier detector was mounted at a backscattering angle of 165°.

5.9. ERROR CALCULATIONS

The given errors for the range distribution and the second moments are calculated from several experimental uncertainties. The total error in the first moment is calculated by taking the following factors into account:

- statistical uncertainty of the maximum
- ≈ 5 % uncertainty in the tabulated values given for stopping
- uncertainty of the surface

The squares of these uncertainties were added to obtain the square of the total experimental error in the first range moment.

The total error from the second range moment was calculated from:

- statistical uncertainties
- ≈ 5 % uncertainty from stopping values, taking only into account the width of the curve.

The uncertainty of the surface channel is not important for the second moment. The squares of the given uncertainties add up to the square of the total error in the second range moment.

5.10. DIFFUSION ANALYSIS

The diffusion coefficients were obtained with the finite difference method using the computer code DIFFUS as described in chapter 2.4. by comparing the NRA depth profiles before and after annealing.

The sensitivity of the applied method to determine diffusion coefficients depends on several experimental parameters. High enough count rates in an energy scan are essential to reduce experimental errors in the obtained range parameters. Small energy step widths of the analysing beam increase the depth resolution. However, for smaller energy steps the total analysing time increases for a sufficient count rate, which can lead to a degradation of the

target surface by the analysing beam already after a few energy scans. For best results the parameters were adjusted to the values mentioned in chapter 5.6.3.

The lower detection limit of diffusion coefficients can be estimated by taking depth distributions of an implanted sample where no detectable diffusion occurred. Experimental uncertainties for the full width at half maximum (FWHM) of the depth distribution are typically about $\Delta x \approx 5\ nm$ for at typical FWHM of 150 to 200 *nm*.

From the change in FWHM of a gaussian depth distribution the diffusion coefficient is calculated to $W^2 = 4\ Dt\ \ln(2) + W_0^2$ [54], where W_0 and W are the widths before and after diffusion, respectively. The total uncertainty Δx_{tot} in the width for an initial and final distribution calculates to: $(\Delta x_{tot}) = [(\Delta x_i)^2 + (\Delta x_f)^2]^{1/2} \approx 7 \times 10^{-7}\ cm$. For an annealing time of 1 hour an upper limit for diffusion coefficients of implanted samples are calculated to: $D_{min} \approx 10^{-15}\ cm^2\ s^{-1}$.

Smaller FWHM of 10-20 *nm* and experimental uncertainties of about $\Delta x = 3\ nm$ in the determination of the FWHM of the thin films are due to smaller energy steps and higher count rates. Total uncertainties in the FWHM are in the range of $\Delta x_{tot} \approx 4\ nm$, which leads to a minimum detection limit for the diffusion coefficient of $D \leq 10^{-16}\ cm^2\ s^{-1}$.